Editors' Suggestion

Toward quantum scaling advantage in approximate optimization

J. Pawłowski,[1] P. Tarasiuk,[2] J. Tuziemski,[2,3] Ł. Pawela,[4,2] and B. Gardas[4]

[1]*Institute of Theoretical Physics, Faculty of Fundamental Problems of Technology, Wrocław University of Science and Technology, 50-370 Wrocław, Poland*

[2]*Quantumz.io Sp. z o.o., Puławska 12/3, 02-566 Warsaw, Poland*

[3]*Institute of Informatics, Faculty of Mathematics, Physics and Informatics, University of Gdańsk, Wita Stwosza 57, 80-308 Gdańsk, Poland*

[4]*Institute of Theoretical and Applied Informatics, Polish Academy of Sciences, Bałtycka 5, 44-100 Gliwice, Poland*

(Received 28 May 2025; revised 8 April 2026; accepted 1 June 2026; published 8 July 2026)

In a recent Letter [H. Munoz-Bauza and D. Lidar, Phys. Rev. Lett. **134**, 160601 (2025)], quantum annealing was reported to exhibit a scaling advantage in approximately solving quadratic unconstrained binary optimization (QUBO) problems. Here, we revisit these findings by employing the simulated bifurcation machine (SBM), a nonlinear dynamical system that exploits chaotic behavior rather than thermal fluctuations. Our approach originates from quantum dynamics and shares key operational features with quantum annealing: (i) nearly parallel evolution and (ii) a well-defined relation between the energy gap, run-time, and solution quality. We obtain comparable or superior scaling, closing the reported quantum-classical gap. We further show that the small instances studied previously are insufficient to infer asymptotic behavior. Extending the analysis to larger problems reveals robust classical performance, indicating that current quantum annealers are unlikely to exhibit a clear scaling advantage over SBM-like solvers on quantum-annealing-correction-type QUBO problems under the run-time accounting studied here. Finally, we identify sparse problem classes where future quantum devices could achieve a genuine scaling advantage once hardware overheads are mitigated.

DOI: 10.1103/qcws-8kgm

I. INTRODUCTION

A central goal of quantum computing is to demonstrate quantum advantage—tasks where quantum devices outperform classical ones [1,2]. Despite major progress, a clear demonstration remains elusive [3]. Quantum advantage may manifest as reduced complexity, faster run-time, or lower energy use, but any claim must be validated against steadily improving classical algorithms [4–7]. This was evident in random circuit sampling [8], where an initial gap was soon narrowed [9] and later closed [10] by classical methods. For current NISQ devices [11], such claims tend to provoke debate rather than consensus. A similar pattern followed a recent "quantum advantage" claim in physical simulation [12], which prompted rapid advances in tensor-network approaches [13,14] and continued scrutiny [15].

A more recent claim [16] reported a quantum advantage in approximate optimization, where D-Wave quantum annealing was said to outperform the "top classical heuristic algorithm" on quadratic unconstrained binary optimization (QUBO) problems [17]. QUBO is equivalent to the Ising model, $H = -\sum_{i<j} J_{ij} s_i s_j - \sum_i h_i s_i$ with binary spin variables $s_i = \pm 1$, couplings J_{ij}, and local fields h_i. Thus, such problems are naturally suited for quantum annealers [18]. Given their broad practical relevance [19], the claim deserves careful reexamination.

In this Letter, we explain why the reported advantage cannot hold and provide a conceptual foundation for advancing toward genuine quantum advantage in approximate optimization. We examine whether a classical algorithm sharing key features of quantum annealing, namely nearly parallel dynamics and a well-defined relation between the energy gap, run-time, and solution quality, can reproduce similar scaling. The answer is affirmative: the favorable scaling reported in Ref. [16] cannot be uniquely interpreted as quantum advantage. Instead of thermally or stochastically inspired solvers such as PT-ICM, we employ a classical method obtained via a dequantization procedure, the simulated bifurcation machine (SBM) [20]. This approach is based on nonlinear Hamiltonian dynamics and provides a quantum-inspired classical baseline.

Our approach yields scaling comparable to, and in some regimes better than, that of the quantum annealer, removing the previously reported gap to a classical baseline. We further highlight methodological assumptions and finite-size effects in Ref. [16] that biased results toward quantum annealing. Extending the analysis to much larger problems, with up to $N \approx 4 \times 10^4$ variables (requiring a QPU with Pegasus topology and at least 1.5×10^5 physical qubits), we

establish a robust classical baseline for future quantum advantage studies. Finally, we identify sparse instances where quantum annealers can rapidly obtain high-quality solutions and may demonstrate a genuine scaling advantage *once hardware-level run-time limitations are mitigated.*

II. THERMAL VS CHAOTIC VS QUANTUM ANNEALING

The scaling advantage claimed by Ref. [16] is facilitated by the use of quantum-annealing correction (QAC) [21], which considerably improves the quality of the low-energy sampling, at the cost of restricting the number and connectivity of *logical* qubits. To ensure a fair comparison, we first use exactly the same instances as in Ref. [16], available via Harvard Dataverse [22], and later extend the study to additional classes of instances. More precisely, we consider random problems *native to the topology* of the logical QAC graph created from the D-Wave Advantage 4.1 QPU [23]. The couplings are drawn from the Sidon-28 set $\pm\{8/28, 13/28, 19/28, 1\}$, and for each size of the logical graph $L \in \{5, 6, \cdots, 15\}$, we use 125 instances. The number of logical qubits varies from $N = 142$ ($L = 5$) to $N = 1322$ ($L = 15$).

Following Ref. [16], we define the time-to-ε metric as

$$\mathrm{TT}\varepsilon \doteq t_f \cdot \frac{\log(1-0.99)}{\log(1-p_{E\le E_0+\varepsilon|E_0|})}, \tag{1}$$

where t_f is the time taken to generate the sample, and $p_{E\le E_0+\varepsilon|E_0|}$ is the probability of finding a solution with energy E, within the ε optimality gap of the true ground state energy E_0, certified by the Gurobi solver [24]. For each instance, we compute the average run-time t_f and success probability $p_{E\le E_0+\varepsilon|E_0|}$ over 100 independent solver runs. The median of TTε across all instances of size N gives $[\mathrm{TT}\varepsilon]_{\mathrm{Med}}$, and its standard deviation is estimated via bootstrap resampling. For SBM, we distinguish two run times: the total run-time t_f^{tot}, including all overhead from CPU-GPU communication, memory handling, and result aggregation, and the pure GPU run-time t_f^{GPU}, representing the actual compute time (averaged across GPUs when applicable). The latter most closely corresponds to the D-Wave annealing time τ, which omits programming and readout overheads. However, unlike t_f^{GPU}, measured during execution, τ is *preset* and cannot be independently verified afterward—a significant distinction discussed in Sec. S5 of Supplemental Material [25].

As in Ref. [16], we optimize $[\mathrm{TT}\varepsilon]_{\mathrm{Med}}$ over the solver parameters, that is, number of steps N_s and replicas N_r (cf. Methods). The optimal N_s and N_r values are shown in the bottom rows of Fig. 1 for $\varepsilon \in \{0.75, 1.00, 1.10, 1.25\}\%$. For small instances, the larger energy spacing allows smaller N_s and larger N_r to enhance success probability within the optimality gap. As instance size grows, the Hamiltonian must vary more slowly, so typically the optimal N_s increases while N_r decreases, balancing run-time and solution quality.

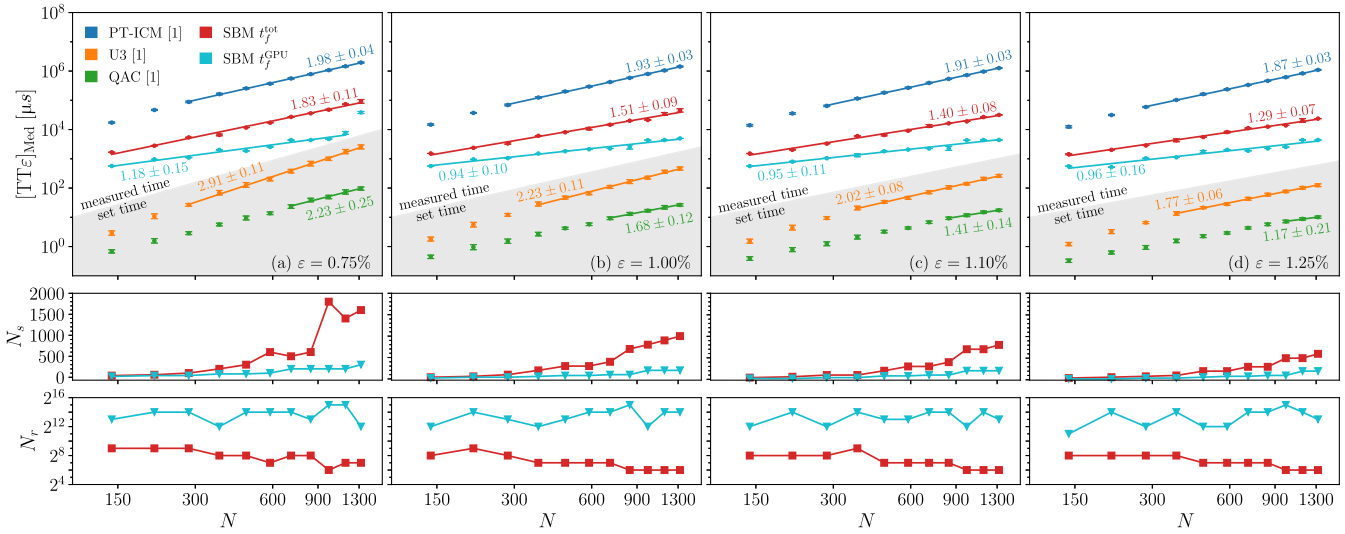

FIG. 1. Time-to-$\varepsilon[\mathrm{TT}\varepsilon]_{\mathrm{Med}}$ scaling with instance size N for Sidon-28 problems. Panels (a)–(d) correspond to target optimality gaps of $\varepsilon \in \{0.75, 1.00, 1.10, 1.25\}\%$. Data for PT-ICM (blue), U3 (orange), and QAC (green) are reproduced from Ref. [16]. Remaining results concern the simulated bifurcation machine (SBM) using one GPU: total run-time t_f^{tot} (red) and pure GPU run-time t_f^{GPU} (cyan). Solid lines show power-law fits $[\mathrm{TT}\varepsilon]_{\mathrm{Med}} \propto N^{\alpha}$, with exponents α indicated. Shading differentiates set-time (shaded) from measured-time (unshaded) data. Even including overheads, GPU-based SBM matches or surpasses PT-ICM, U3, and QAC across all ε, challenging the notion of a quantum scaling advantage. Lower panels display optimal SBM parameters, number of steps N_s and replicas N_r, minimizing $[\mathrm{TT}\varepsilon]_{\mathrm{Med}}$ for each N and ε.

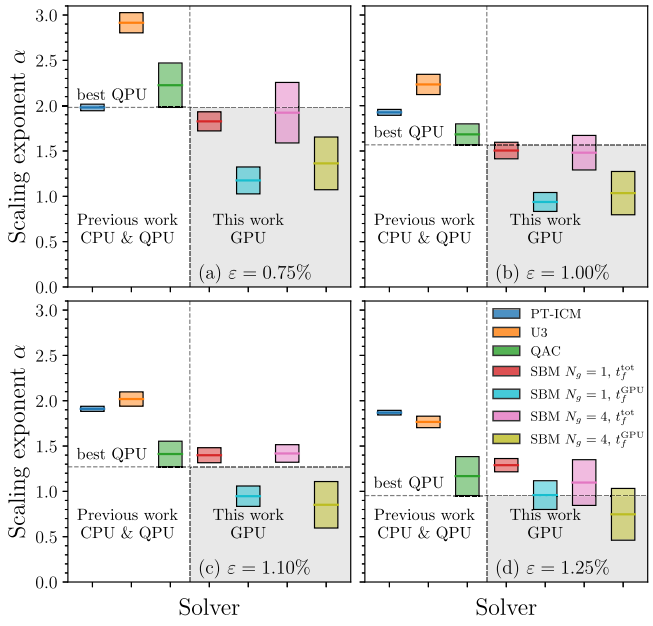

FIG. 2. Time-to-ε scaling exponents α from $[\mathrm{TT}\varepsilon]_{\mathrm{Med}} \propto N^{\alpha}$ for various solvers and $\varepsilon \in \{0.75, 1.00, 1.10, 1.25\}\%$ in panels (a)–(d). Vertical solid lines show α values from fits in Fig. 1, with colored bands indicating ± 2 standard deviations. A vertical dashed line separates CPU/QPU results from Ref. [16] (left) and our GPU-based results (right). The horizontal dashed line marks the best QAC fit, defining the approximate quantum-advantage boundary. Lightly shaded regions highlight cases closing the quantum–classical gap—SBM $(t_f^{\mathrm{tot}}, N_g = 1)$ (red, up to $\varepsilon \approx 1\%$), as well as $(t_f^{\mathrm{GPU}}, N_g = 1)$ (cyan) and both $N_g = 4$ cases (pink and light green) for all ε.

In the top row of Fig. 1, we present $[\mathrm{TT}\varepsilon]_{\mathrm{Med}}$ scaling for the GPU-based SBM alongside the original PT-ICM, U3, and QAC results from Ref. [16]. Data are shown on a log-log scale with solid lines representing power-law fits $[\mathrm{TT}\varepsilon]_{\mathrm{Med}} \propto N^{\alpha}$. As expected, polynomial scaling fails at $\varepsilon = 0$, since exact discrete optimization is NP-hard [32]. The resulting exponents α are summarized in Fig. 2, showing that SBM with $N_g = 1$ and t_f^{tot} yields scaling comparable to, or smaller than, the best QAC results for all ε. These findings already challenge the claim of quantum scaling advantage. When considering pure GPU run-time t_f^{GPU} (analogous to the annealing time τ), the gap closes further, underscoring how strongly the fitted exponents depend on overhead in the small-instance regime. Exploiting SBM's parallelism, we also ran $N_g = 4$ GPUs, enabling larger N_r without increasing t_f^{GPU}; the corresponding exponents are shown in Fig. 2 (see also Sec. S1 of Supplemental Material [25]).

Finally, to probe the asymptotic scaling of $[\mathrm{TT}\varepsilon]_{\mathrm{Med}}$, we extend our analysis to systems far beyond the current

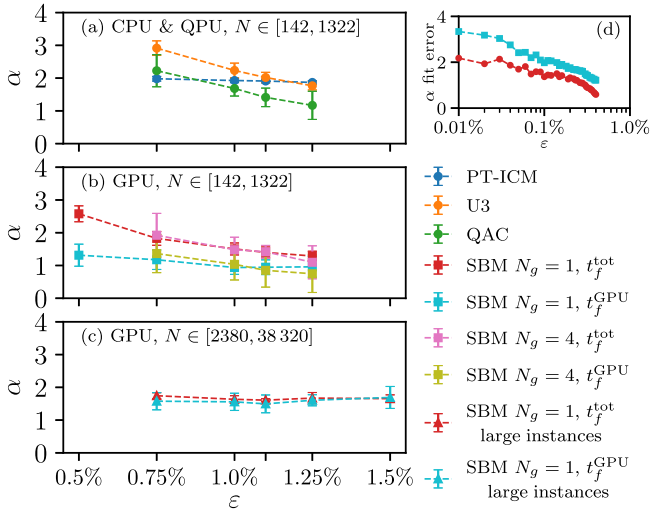

FIG. 3. Dependence of the scaling exponent α on the optimality gap ε for small (a),(b) and large instances (c). For larger systems, scaling is more stable and overhead effects nearly vanish. However, α is expected to diverge as $\varepsilon \to 0$, marking the transition from power law to exponential $[\mathrm{TT}\varepsilon]_{\mathrm{Med}}$ scaling. Panel (d) confirms this, showing the power-law fit error rising rapidly as $\varepsilon \to 0$.

capabilities of quantum annealers, with sizes ranging from $L = 20\,(N = 2380)$ to $L = 80(N = 38\,320)$. The dependence of the scaling exponent α on the optimality gap ε, extracted from these larger systems, is shown in Fig. 3(c). The scaling becomes noticeably more robust, with overhead effects essentially vanishing. See Sec. S2 of Supplemental Material [25] for details.

III. TOWARD QUANTUM SCALING ADVANTAGE

A more plausible route to quantum scaling advantage is to focus on instance classes for which information can propagate more efficiently on the annealer than in SBM-like classical dynamics. We therefore study 3D spin-glass instances for which the annealer attains high-quality solutions within the nanosecond-scale fast annealing regime [33,34]. As shown in Fig. 4, when run-time is proxied by the annealing time, τ, the annealer exhibits superior scaling in the $\varepsilon \leq 1\%$ regime (see also Sec. S6 of Supplemental Material [25] for details). Current devices cannot yet demonstrate a true quantum scaling advantage, as realistic overheads (programming, readout, etc.) erase the favorable scaling. Nevertheless, the SBM's inability to reproduce the annealer's scaling exponent using τ as a run-time proxy suggests a promising path toward achieving such an advantage once hardware limitations are mitigated (cf. Sec. S5 in Supplemental Material [25]).

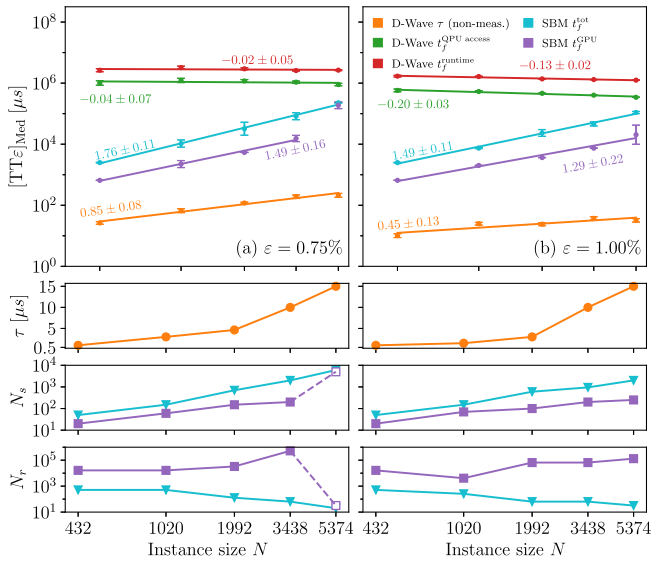

FIG. 4. Time-to-ε ($[\text{TT}\varepsilon]_{\text{Med}}$) scaling for 3D spin glasses [33,34], executed on the D-Wave quantum annealer and the SBM on a single GPU under different time-accounting schemes. Due to D-Wave's topology, embedded 3D instances (chains of length 2, ×2 qubit overhead) were used, while SBM runs directly on the cubic lattice. Results for $\varepsilon \in \{0.75, 1.0\}\%$ are shown in panels (a) and (b), corresponding to the regime of nontrivial power-law scaling. Lower panels show optimal parameters minimizing $[\text{TT}\varepsilon]_{\text{Med}}$; open symbols indicate that for given N, optimal value most likely lies outside the search range. Such points are excluded from fits. SBM results are shown for total run-time $t_f^{\text{run-time}}$ (cyan) and GPU run-time t_f^{GPU} (purple). Orange, green, and red points denote annealing time [16], QPU access, and total run-time, respectively. The nonmeasurable annealing time yields smaller exponents α, but proper time accounting removes this apparent advantage: for $t_f^{\text{run-time}}$ and $t_f^{\text{QPU access}}$, scaling exponents are near zero, indicating that asymptotic scaling is inaccessible in this size regime. Nevertheless, future devices reducing overhead could still realize a genuine quantum advantage.

IV. METHODS: CHAOTIC DYNAMICS

We consider the SBM with discretized Ising interactions governed by [35]:

$$\dot{x}_i = \Delta y_i, \qquad \dot{y}_i = -[\Delta - p(t)]x_i + \xi_0 G(x), \qquad (2)$$

with $G(x) = \sum_{j=1}^{N} J_{ij} f(x_j) + h_i$, where $f(x) = \text{sign}(x)$ is the sign function. We augment the original formulation of dSB with a ternary discretization scheme [36]. Specifically, we replace sign function by $\Theta(|x| - g(t))\cdot \text{sign}(x)$, where $g(t) = 0.7\,\frac{t}{T}$, with T the total time, and $\Theta(x)$ the step function.

The system's nonlinearity arises from a boundary at $|x_i| = \sqrt{2}$. Exceeding this bound forces $x_i \to \sqrt{2}\,\text{sign}(x_i)$ and sets $y_i = 0$. We use $\Delta = 1$ and $\xi_0 = \frac{0.7\Delta}{\sigma\sqrt{N}}$, with σ the standard deviation of the off-diagonal elements of J. The linear schedule $p(t) = t/T$ drives the system through a sequence of bifurcations. Beyond the $p(t) = p_0 = \Delta$ point, the energy landscape approximates that of the Ising Hamiltonian, guiding convergence toward low-energy solutions, which are read out as $s_i = \text{sign}(x_i)$. The algorithm has three hyperparameters: the time step Δt, the number of steps N_s ($T = N_s \Delta t$), and the number of replicas N_r. The schedule $p(t)$ varies slowly from 0 to p_0, with N_s determining the slope of the ramp. See Sec. S4 of Supplemental Material [25] for additional details on the algorithm and its implementation.

V. DISCUSSION AND CONCLUSIONS

We show that chaotic dynamics in nonlinear Hamiltonian systems, as realized in SBM, rather than thermal fluctuations as in classical annealing, close the quantum–classical scaling gap in approximate QUBO optimization reported in Ref. [16]. We further demonstrate that such quantum advantage claims are highly sensitive to run-time definitions, rendering scaling analyses at small system sizes ($L < 20$) unreliable.

The available evidence does not permit a definitive attribution of the observed scaling to purely quantum effects. Our results, together with those of Ref. [16], support several interpretations, including that the D-Wave device operates in a mixed regime where classical and quantum processes coexist. In this regime, efficient exploration of low-energy configurations persists for $\varepsilon \lesssim 1.25\%$, producing scaling trends comparable, though not identical, to SBM-like dynamics. This is not necessarily the case for other quantum-inspired, yet classical,

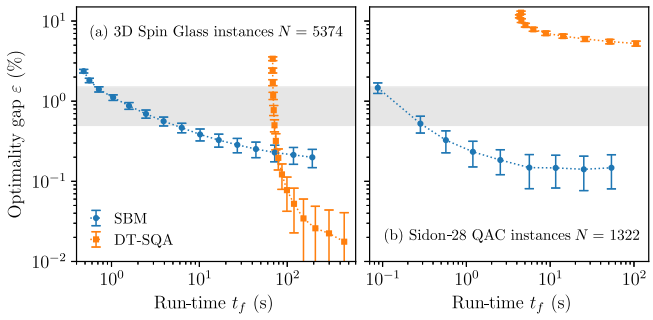

FIG. 5. Average optimality gap ε achieved by SBM and DT-SQA vs measured run-time for (a) 3D spin-glass instances ($N = 5374$) and (b) Sidon-28 QAC instances ($N = 1322$). Averages were taken over 20 instances × 20 runs for (a) and 25 instances × 5 runs for (b). For Sidon-28, DT-SQA fails to reach the target range $\varepsilon \in [0.5, 1.5]\%$ (gray area) and thus cannot show an advantage in time-to-ε scaling. For 3D spin glasses, DT-SQA attains high-quality solutions but with much longer run times than SBM, owing to limited parallelizability [34]. Both methods use embedded 3D instances, where the cubic lattice is minor-embedded into the Pegasus topology with chain length 2 [33,34].

methods, e.g. discrete-time simulated quantum annealing (DT-SQA) [34], cf. Fig. 5.

In QAC, execution time is fixed rather than measured, limiting the operational meaning of TTε in Eq. (1). Nevertheless, chaotic-like dynamics performs comparably or better even under such unfavorable conditions (cf. Fig. 2). For larger systems, different timing definitions yield consistent results (cf. Sec. S2 in Supplemental Material [25]) confirming the robustness of the asymptotic behavior and providing a benchmark for future QPU studies—although realizing this may require hybrid quantum-classical approaches [37].

Furthermore, meaningful quantum advantage in approximate discrete optimization should be evaluated across diverse problem instances (varying in density, size, and structure), and more importantly, as close to $\varepsilon \approx 0$ as possible. Relaxing the advantage criterion to sparse instances and large ε values is designed to favor QPUs. However, SBM-like methods are naturally suited to such simulations, without requiring further modification, whereas current QPU architectures appear fundamentally constrained in this regime. *On the problem classes and under the run-time definitions considered here, current-generation QPUs are therefore unlikely to exhibit a clear scaling advantage over classical solvers*.

Finally, for tailored problems such as 3D spin glasses, the annealer achieves high-quality solutions within the fast annealing regime, exhibiting better apparent *scaling* than classical methods when annealing time is used as a proxy for run-time (cf. Fig. 4). These results delineate the conditions under which next-generation quantum annealers could achieve a genuine, though limited, scaling advantage.

ACKNOWLEDGMENTS

This work was supported by the National Science Center (NCN), Poland, via project Sonata Bis 10, No. 2020/38/E/ST3/00269 (B. G.). Quantumz.io Sp. z o. o. acknowledges support received from The National Centre for Research and Development (NCBR), Poland, via Project No. POIR.01.01.01-00-0061/22.

DATA AVAILABILITY

The data that support the findings of this article are available from the authors upon reasonable request.

[1] A. W. Harrow and A. Montanaro, Quantum computational advantage, Nature (London) **549**, 203 (2017).

[2] S. Boixo, S. V. Isakov, V. N. Smelyanskiy, R. Babbush, N. Ding, Z. Jiang, M. J. Bremner, J. M. Martinis, and H. Neven, Characterizing quantum advantage in near-term devices, Nat. Phys. **14**, 595 (2018).

[3] A. Morvan *et al.*, Phase transitions in random circuit sampling, Nature (London) **634**, 328 (2024).

[4] Y. Zhou, E. M. Stoudenmire, and X. Waintal, What limits the simulation of quantum computers?, Phys. Rev. X **10**, 041038 (2020).

[5] A. Tanggara, M. Gu, and K. Bharti, Classically spoofing system linear cross entropy score benchmarking, arXiv:2405.00789.

[6] D. Aharonov, X. Gao, Z. Landau, Y. Liu, and U. Vazirani, A polynomial-time classical algorithm for noisy random circuit sampling, in *Proceedings of the 55th Annual ACM Symposium on Theory of Computing, STOC '23* (ACM, 2023).

[7] J. Tindall, M. Fishman, E. M. Stoudenmire, and D. Sels, Efficient tensor network simulation of IBM's Eagle kicked Ising experiment, PRX Quantum **5**, 010308 (2024).

[8] F. Arute *et al.*, Quantum advantage using a programmable superconducting processor, Nature (London) **574**, 505 (2019).

[9] Y. A. Liu *et al.*, Closing the "quantum advantage" gap: Achieving real-time simulation of a random quantum circuit using a new Sunway supercomputer, in *Proceedings of the International Conference for High Performance Computing, Networking, Storage and Analysis, SC'21* (Association for Computing Machinery, New York, 2021).

[10] F. Pan, K. Chen, and P. Zhang, Solving the sampling problem of the Sycamore quantum circuits, Phys. Rev. Lett. **129**, 090502 (2022).

[11] J. Preskill, Quantum computing in the NISQ era and beyond, Quantum **2**, 79 (2018).

[12] A. D. King *et al.*, Beyond-classical computation in quantum simulation, Science **388**, 199 (2025).

[13] J. Tindall, A. F. Mello, M. Fishman, E. M. Stoudenmire, and D. Sels, Dynamics of disordered quantum systems with two- and three-dimensional tensor networks, Science **392**, 868 (2026).

[14] L. Mauron and G. Carleo, Challenging the quantum advantage frontier with large-scale classical simulations of annealing dynamics, arXiv:2503.08247.

[15] A. D. King *et al.*, Comment on: "Dynamics of disordered quantum systems with two- and three-dimensional tensor networks" arXiv:2503.05693, arXiv:2504.06283.

[16] H. Munoz-Bauza and D. Lidar, Scaling advantage in approximate optimization with quantum annealing, Phys. Rev. Lett. **134**, 160601 (2025).

[17] F. Glover, G. Kochenberger, R. Hennig, and Y. Du, Quantum bridge analytics I: A tutorial on formulating and using QUBO models, Ann. Oper. Res. **314**, 141 (2022).

[18] K. Boothby, A. D. King, and J. Raymond, Zephyr topology of D-wave quantum processors (2021). accessed: 2025-01-31.

[19] G. Kochenberger, J.-K. Hao, F. Glover, M. Lewis, Z. Lü, H. Wang, and Y. Wang, The unconstrained binary quadratic programming problem: A survey, J. Comb. Optim. **28**, 58 (2014).

[20] H. Goto, Bifurcation-based adiabatic quantum computation with a nonlinear oscillator network, Sci. Rep. **6**, 21686 (2016).

[21] K. L. Pudenz, T. Albash, and D. A. Lidar, Error-corrected quantum annealing with hundreds of qubits, Nat. Comm. **5**, 3243 (2014).

[22] H. Munoz Bauza and D. Lidar, Scaling advantage in approximate optimization with quantum annealing spin-glass instances, Phys. Rev. Lett. **134**, 160601 (2025).
[23] D.-W. S. Inc., Advantage system4.1 solver properties (2025). accessed: 2025-11-07.
[24] Gurobi Optimization, LLC, Gurobi Optimizer Reference Manual (2024).
[25] See Supplemental Material at http://link.aps.org/supplemental/10.1103/qcws-8kgm, including Refs. [26–31] for details of the SBM algorithm, its properties, multi-GPU performance, and large-instance scaling. It also discusses scaling behavior, run-time accounting, and additional 3D spin-glass results and summarizes the hardware used.
[26] J. Pawlowski, J. Tuziemski, P. Tarasiuk, A. Przybysz, R. Adamski, K. Hendzel, L. Pawela, and B. Gardas, VeloxQ: A fast and efficient QUBO solver, arXiv:2501.19221.
[27] H. Goto, K. Tatsumura, and A. R. Dixon, Combinatorial optimization by simulating adiabatic bifurcations in nonlinear Hamiltonian systems, Sci. Adv. **5**, eaav2372 (2019).
[28] J. Wang, D. Ebler, K. Y. M. Wong, D. S. W. Hui, and J. Sun, Bifurcation behaviors shape how continuous physical dynamics solves discrete Ising optimization, Nat. Commun. **14**, 2510 (2023).
[29] F. Ghimenti, A. Sriram, A. Yamamura, H. Mabuchi, and S. Ganguli, The geometry and dynamics of annealed optimization in the coherent Ising machine with hidden and planted solutions, arXiv:2510.21109.
[30] A. Soriani, P. Nazé, M. V. S. Bonança, B. Gardas, and S. Deffner, Three phases of quantum annealing: Fast, slow, and very slow, Phys. Rev. A **105**, 042423 (2022).
[31] D.-W. S. Inc, Operation and timing (2025), [accessed October 24, 2025], https://docs.dwavequantum.com/en/latest/quantum_research/operation_timing.html.
[32] A. Lucas, Ising formulations of many NP problems, Front. Phys. **2**, 74887 (2014).
[33] A. D. King *et al.*, Quantum critical dynamics in a 5,000-qubit programmable spin glass, Nature (London) **617**, 61 (2023).
[34] S. Chowdhury *et al.*, Pushing the boundary of quantum advantage in hard combinatorial optimization with probabilistic computers, Nat. Commun. **16**, 9193 (2025).
[35] H. Goto, K. Endo, M. Suzuki, Y. Sakai, T. Kanao, Y. Hamakawa, R. Hidaka, M. Yamasaki, and K. Tatsumura, High-performance combinatorial optimization based on classical mechanics, Sci. Adv. **7**, eabe7953 (2021).
[36] T. Zhang and J. Han, Quantized simulated bifurcation for the Ising model, in *Proceedings of the 2023 IEEE 23rd International Conference on Nanotechnology (NANO)* (2023), pp. 715–720.
[37] D-Wave, D-wave hybrid framework (2025), [accessed: January 30, 2025], https://docs.dwavequantum.com/en/latest/ocean/api_ref_hybrid/index.html.